Defect Printability Study using EUV Lithography

Christian Holfeld[1§], Karsten Bubke[1], Falk Lehmann[1], Bruno La Fontaine[2], Adam R. Pawloski[2], Siegfried Schwarzl[3], Frank-Michael Kamm[3], Thomas Graf[4], Andreas Erdmann[4]

[1]Advanced Mask Technology Center, Raehnitzer Allee 9, 01109 Dresden, Germany
[2]Advanced Micro Devices, One AMD Place, Sunnyvale CA 94088-3453, USA
[3]Infineon Technologies, Koenigsbruecker Strasse 180, 01079 Dresden, Germany
[4]Fraunhofer Institute of Integrated Systems and Device Technology, Schottkystrasse 10, 91058 Erlangen, Germany

ABSTRACT

Defect-free masks are one of the top issues for enabling EUV lithography at the 32-nm node. Since a defect-free process cannot be expected, an understanding of the defect printability is required in order to derive critical defect sizes for the mask inspection and repair. Simulations of the aerial image are compared to the experimental printing in resist on the wafer. Strong differences between the simulations and the actual printing are observed. In particular the minimum printable defect size is much larger than expected which is explained in terms of resist resolution. The defect printability in the current configuration is limited by the resist process rather than the projection optics.

Keywords: EUV lithography, defect, defect printability, critical defect size, resist resolution

1. INTRODUCTION

Heading towards the 32-nm node, one option for the pattern generation of the electronic circuits on wafer is Extreme Ultraviolet (EUV) lithography. Using radiation with the extremely short wavelength of 13.5 nm offers the opportunity to relax the very complex mask patterns by avoiding much of the sub-resolution assist features required for 193-nm lithography at a comparable design rule. However, the change to EUV lithography will require the adoption of new techniques like reflective masks, pellicle-less systems and vacuum operation.

The development of the EUV technology still encounters several fundamental problems. Between the top challenges are appropriate resists with high resolution, high sensitivity and low line-edge roughness and the availability of defect-free masks. There are predictions of what size of defects are critical and will print but this remains to be confirmed by experiment. A critical mask defect size predicted by the ITRS roadmap 2005 is 26 nm at 32-nm node [1].

The critical defect size typically is derived from a printing study for individual defect types which takes the full lithographic process into account (illumination, resist process, etc.). So far only a few experimental studies were done [2-4]. These studies were carried out at the experimental exposure tools (10x EUV Microstepper, ETS full-field scanner) already some years ago. A critical defect size was reported as small as 15 nm on mask for long extensions which in fact corresponds to a CD variation of the feature. Absorber point defects are much more appropriate since they better represent small native defects expected on mask.

This study aims on doing a state-of-the art printability study for absorber defects in order to learn about the printing behavior of different kinds of defects and possibly derive a critical defect size. A learning about the critical defect size will have a great impact on the specification and development of inspection and repair processes in order to ensure defect-free masks. The experimental results are compared to simulations of the aerial image which allows the separation of effects originating in the projection optics and the wafer resist process.

§ E-mail: christian.holfeld@amtc-dresden.com, Phone : +49 (351) 4048 373

Emerging Lithographic Technologies X, edited by Michael J. Lercel,
Proc. of SPIE Vol. 6151, 61510U, (2006) · 0277-786X/06/$15 · doi: 10.1117/12.656386

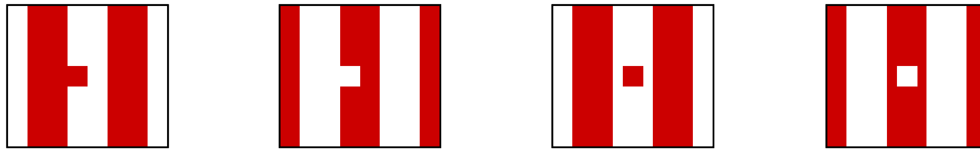

Fig. 1: Schematic view of the dark and clear defect types discussed in this paper. From left to right: line extension (dark), intrusion (clear), centered dark and centered clear.

2. DEFECT TYPES AND SIZE DEFINITION

This study is restricted to absorber point defects. Point defects are considered here as defects with similar dimensions in all directions which seems to be the best representation of small native defects with a size in the order of critical defects. The point defects are emulated by programmed defects on the mask corresponding to squares in the layout. The defects are inserted in a dense line/space pattern with duty cycle 1:1 and a pitch of 120 nm on wafer (300nm half pitch on mask). This feature size of the line/space pattern was chosen since earlier printing studies have shown a reasonable size of the process window with the same lithographic process [5]. Only a vertical orientation of the line/space pattern was investigated corresponding to a geometry in which the oblique incidence of the EUV light on the mask is oriented along the lines and no shadowing effect is expected.

Four different defect types were programmed both in dark and clear tone (see Fig. 1). One class of defects comprises extensions or intrusions of an absorber line which directly change the local dimension of this line. A second class of defects refers to a small area of absorber or a hole centered to a space or line, respectively. Please note that although these defects are placed in a non-shadowed line/space pattern, the defects themselves are subject to shadowing along the vertical direction. The shadowing leads to an increase of the effective vertical dimension for dark defects and a decrease for clear defects.

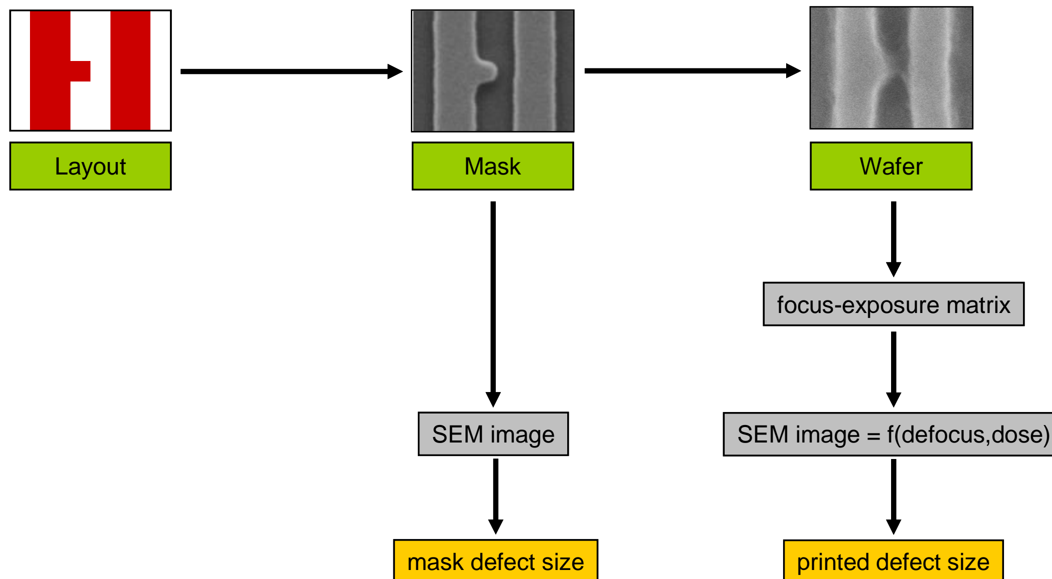

Fig. 2: Scheme for the measurements of defect sizes on mask and wafer. Only measured values are used in this printability study.

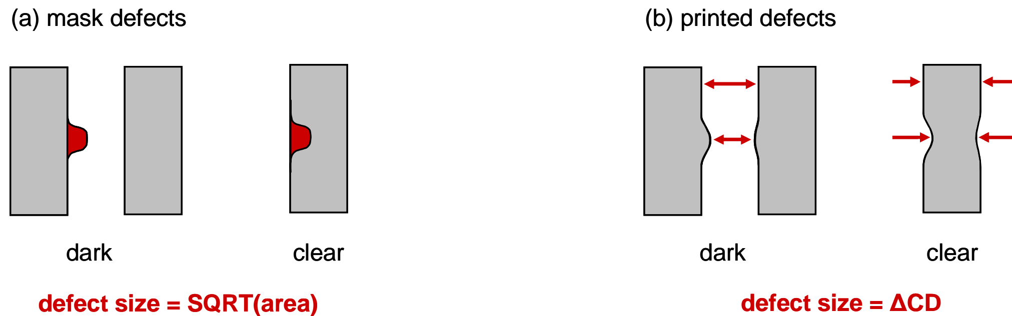

Fig. 3: Definition of defect size for mask original and printed defect: The mask defect is characterized by an area-equivalent size and the printed defect is given by a change of feature CD.

Since the shape of the defects is modified during the pattern transfer of the layout onto the mask and once again during the printing of the mask, it is necessary to discuss what characteristic dimension of the defect determines the defect size. See also Figs. 2 and 3 for this discussion. All defect sizes discussed in this paper are measured from actual SEM images taken from mask or from wafer, i.e. no nominal defect size from the layout is used. From printing studies with DUV wavelength it is a well known fact that for printability only the area of defect matters and not its actual shape. This is supported by test simulations. The defect size on mask is therefore defined as the area-equivalent dimension calculated as the square root of the defect area measured from a SEM image of the actual defect. Throughout this paper, all mask defect sizes are given on mask scale (5x).

On wafer, the actual change of the line or space CD due to the defect printing is more relevant. Thus, the defect size is taken as the difference of the space CD (dark defects) or line CD (clear defects) at the position of the defect and at a defect-free site. Particularly for centered defects, both edges of these features are influenced in printing by the defects. This effect is intrinsically included in our approach. Most defect sizes on wafer are measured at best focus and best dose unless explicitly stated.

3. EXPERIMENTAL CONDITIONS

The experimental wafer printing was carried out at the Micro Exposure Tool (MET) at the Lawrence Berkeley National Laboratory (LBNL). The MET is a small-field printing tool which uses undulator radiation from the ALS synchrotron as source. The light is incident on the mask surface with an angle of 3.6° off the normal. The illuminator pupil is fully programmable and allows for arbitrary illumination schemes. Demagnification of the image is by a factor of five which is different to the upcoming full-field tools. The particular setup of the MET tool has been described elsewhere [6].

The mask used for the defect printability study had a TaN/SiO2 absorber stack with a total thickness of 55 nm. The mask was printed with an annular illumination with an inner and outer sigma of 0.3 and 0.6, respectively. The annular illumination scheme is invariant to rotation and thus does not prefer any orientation on the mask except the unavoidable difference between the shadowed and non-shadowed features due to the off-normal illumination of the mask. Numerical aperture was 0.3 on wafer side corresponding to 0.06 on the mask side.

The patterns were printed in MET-1K from Rohm and Haas which is a positive-type, chemically amplified resist. At the time of printing, this resist showed the best performance in terms of simultaneous high resolution, good sensitivity and low LER. Thickness was 125 nm and the resist process followed the baseline process established at the LBNL. Using annular illumination, a resolution of 30-40 nm was demonstrated with this resist [7,8]. Practically, a focus-exposure matrix (FEM) was printed with focus steps of 50 nm and dose steps of 5%. The position of best focus and best dose within the FEM was determined from SEM images of the target pattern with a dose-to-size of 60 nm for the half pitch of the dense lines (duty cycle 1:1).

4. SIMULATIONS

The simulations were performed at the Fraunhofer Institute IISB with an in-house software. These simulations are configured as direct comparison of the aerial image to the experimental results. The simulation parameters were taken from the experimental conditions and were set to the following values: wavelength = 13.4 nm, NA = 0.3, 5x demagnification, 4.0° angle of incidence and annular illumination with an inner and outer sigma of 0.3 and 0.6, respectively. The defect sizes were those measured on the mask. For the sake of simplicity, the simulations used geometrical squares instead of the smoothed shape observed on mask. However, we found only negligible influence of the defect width/height ratio as long as the area is maintained.

The simulation procedure involved the rigorous computation of the light diffraction from the EUV masks in the near field and transformation of the near field into the aerial image in terms of Fourier optics. For the CD evaluations, a threshold model was applied to the aerial image. The dose-to-size was determined in order to obtain a 60 nm (1:1) dense line/space pattern. The light diffraction from the EUV masks computed by splitting the light propagation domain in two parts: the absorber stack which defines the features on the mask, and the multilayer reflecting the light. The absorber stack is modeled by a time-domain finite difference method (FDTD) and the reflectivity of the multilayer is computed with a transfer-matrix method [9]. Amplitude and phase of the light directly above the absorber, computed with FDTD and transfer matrices as described before, are used to construct a thin-mask equivalent, producing the same light distribution and characterized by a complex valued transmission ("Virtual thin mask"). This thin mask serves as input for all aerial-image simulations.

The numerical grid resolution for the FDTD calculations was set to 1nm. The optical constants for the different mask materials were taken from the web site of the Center for X-Ray Optics [10]. The simulations were performed for a mask pattern of 60 nm lines/spaces (wafer scale) with a duty cycle of 1:1 (120 nm pitch). No flare was included in the simulations. A linear flare vs dose distribution does not influence the simulated defect size (shift of the aerial image to higher intensities only) and a non-linear model would be required for any better match to the experiment.

5. DEFECT PRINTABILITY IN AERIAL-IMAGE SIMULATIONS

Given the measured defect size on mask, simulations of the 3D aerial images of line extensions and intrusions were carried out. The defects were approximated by squares with the same area as those on mask. A threshold model was applied leading to 60 nm half pitch (dose-to-size). The defect size was then evaluated as CD difference in the same way than for the experimental data. The results are shown in Fig. 4.

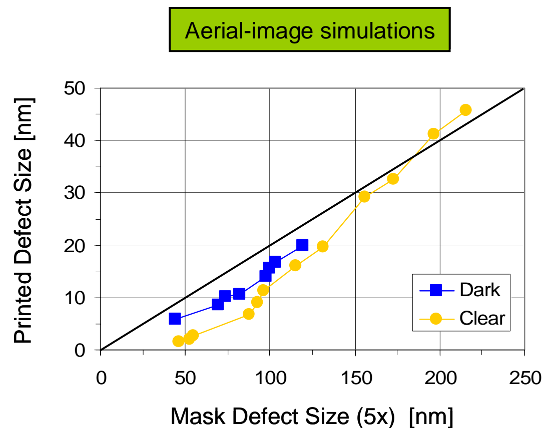

Fig. 4: Printed defect size vs mask defect size for absorber line extensions and intrusions as derived from simulations of the aerial image. The black line indicates the ideal demagnification by a factor of five.

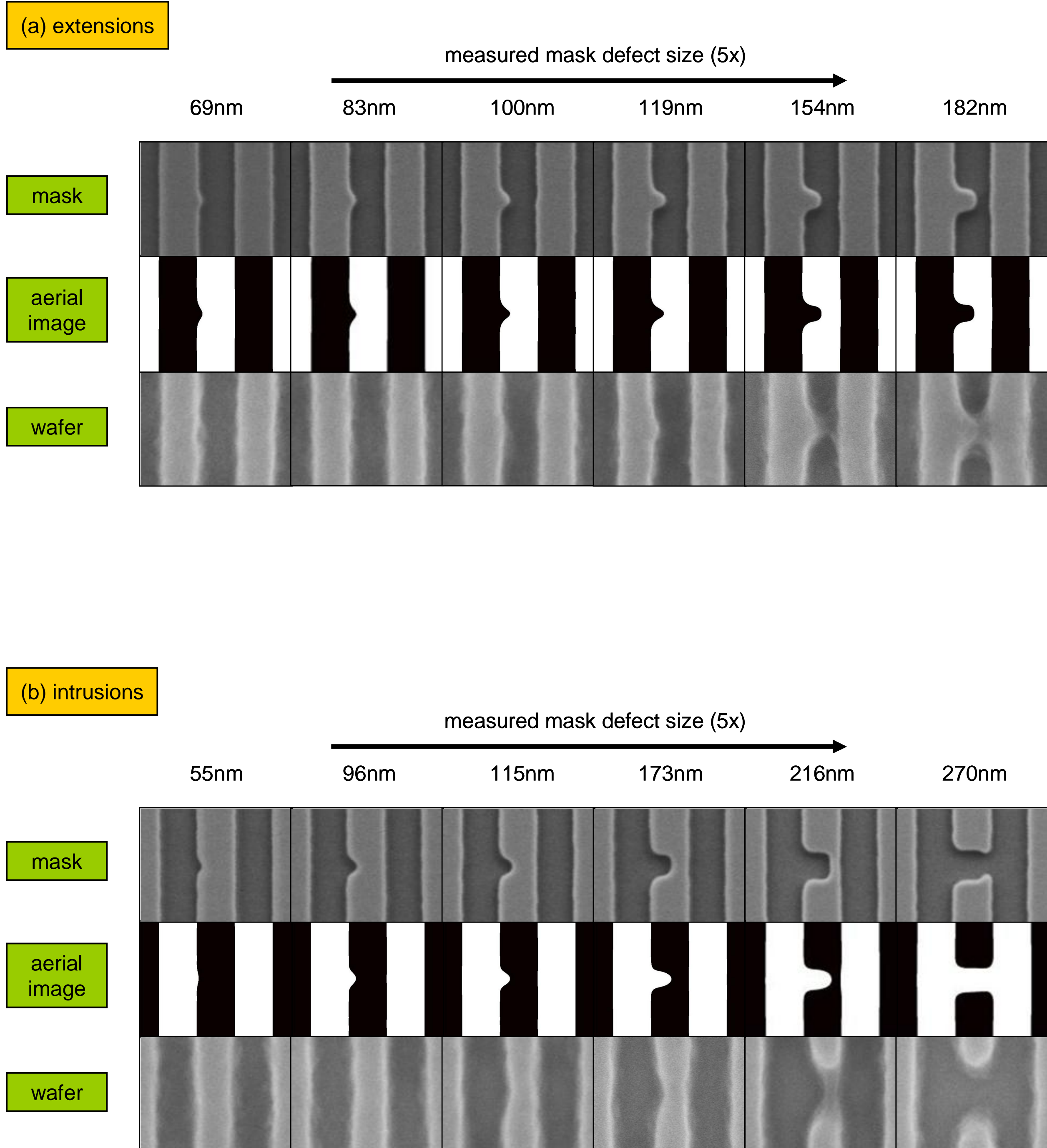

Fig. 5: Defect images through size for (a) extensions and (b) intrusions of a 60 nm dense absorber line (wafer scale). The images show the original mask defect (top row), simulated aerial images (middle) and printed defect in resist (bottom row). The defect size is the measured mask defect size on mask scale (5x).

The printed defect size grows approximately linearly with the mask defect size. However, the defect size in the aerial image is smaller than expected from the ideal demagnification of 5x indicated by the black line. Particularly at small mask defects, the extensions are larger (more critical) than the intrusions. This trend can be attributed to a shadowing effect for the defects which reduces (increases) the effective defect area for clear defects (dark defects) at the same mask defect size.

From these data, a critical defect size can be extrapolated by a linear fit. For a maximum CD deviation of 6 nm (corresponding to the widely used 10% criterion of acceptable CD variations) a critical defect size of 50 nm for line extensions and 75 nm for intrusions can be derived at the 60 nm design rule. This critical defect size is naturally reduced for smaller design rules. If the defect printability data derived from 60 nm lines/spaces are extrapolated down to the 32-nm design rule (though it is not fully correct to do so) the critical size would be reduced to 37 nm or 63 nm, respectively, which is larger than the predictions of the ITRS 2005 roadmap [1].

6. EXPERIMENTAL DEFECT PRINTABILITY IN RESIST

The printability of a defect as a function of its size was assessed by analyzing SEM images of these defects in the fields printed at best dose and best focus. It is now useful to compare the experimental resist images with the associated mask images and simulated aerial images. These images through defect size in a 60-nm line/space pattern (wafer scale) are shown in Fig. 5 for the extension and intrusion defects.

The defect shapes on mask and in the aerial image are very similar to each other. It seems that the mask defects are almost identically transferred into the aerial image by the projection optics. A limitation of high spatial frequencies (rounding of corners) by the optics is not observed here since the defect shape is already somewhat smoothed by the mask manufacturing. The similarity in the aerial image holds for both extensions and intrusions. Note that the vertical dimension of the intrusion is compressed with respect to the mask defect due to the shadowing effect.

In contradiction to the aerial image, the appearance of defects in the wafer resist is much different. Small defects cannot be observed in the resist, and there is a bridging of the space or line break for larger defects. Defects close to bridging or line break show a footing of the resist which will generate a faulty pattern transfer during a subsequent etch step. Nevertheless, such footing is not taken into account for the determination of defect size. In contrast to the aerial-image simulations, the defect shape is stretched in vertical direction with respect to the mask image for both extensions and intrusions.

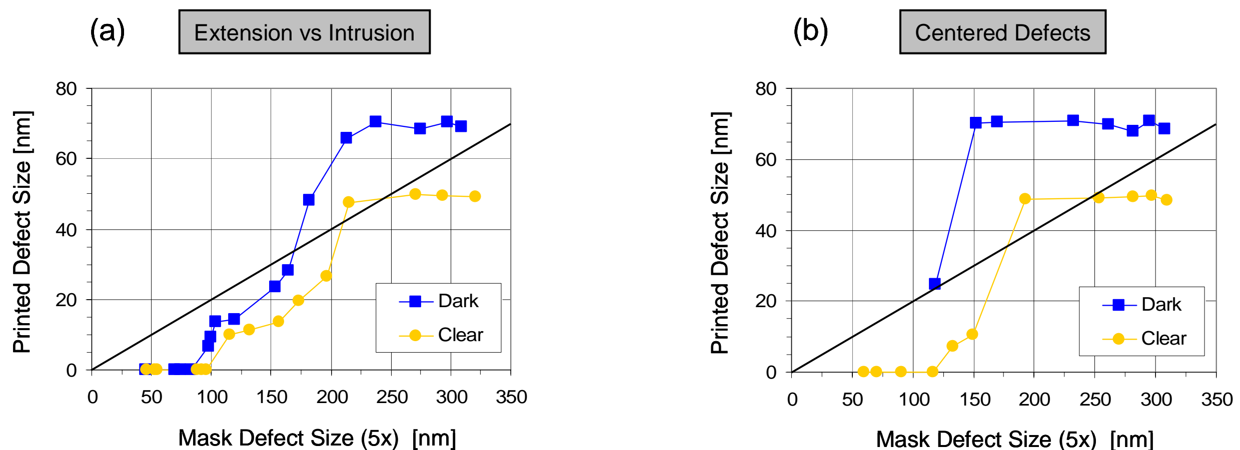

Fig. 6: Printed defect size vs mask defect size as derived from actual wafer printing. The black line indicates the ideal demagnification by a factor of five. (a) absorber line extensions/intrusions and (b) centered defects

Figure 6 shows the actual defect size (change in critical dimension) measured in SEM images of the defects printed in resist. Three different regions can be identified. First, there is a sharp printability limit around a mask defect size of 100 nm (mask scale). Defects on mask smaller than that do not show up in the resist image. This is the most striking difference to the aerial image simulations. In the second region, defects larger than the printability limit grow in printed defect size in accordance with a growing mask defect size. At the same mask defect size, the CD change of the line or space feature (i.e. the printed defect size) is larger for extensions than for intrusions. This result confirms the prediction from the simulation. Finally, bridging or line breaks are observed for defects larger than 150-200 nm mask defect size since the gap between the defect and the adjacent line or space, respectively, is too small. Before the bridging or line break actually occurs there is a certain transition region where the defects grow faster than they would do in a semi-dense pattern due to interaction with the next feature. Centered defects do not show the second region since they switch almost immediately from the non-printing to the bridging/line break behavior.

The defect size in the third region is by definition set to the CD of the line or space feature, respectively. Thus, this region should show up as a plateau. These plateaus have a difference of approximately 20 nm due to uncertainties in the edge detection in the SEM image and deviations from the target duty cycle but the value of the pitch is conserved (120 nm pitch). This difference does affect only the third region since bridging or line break measurements are based on the detection of a left and a right feature edge whereas all other measurements of the defect size detect a difference between the same type of edge.

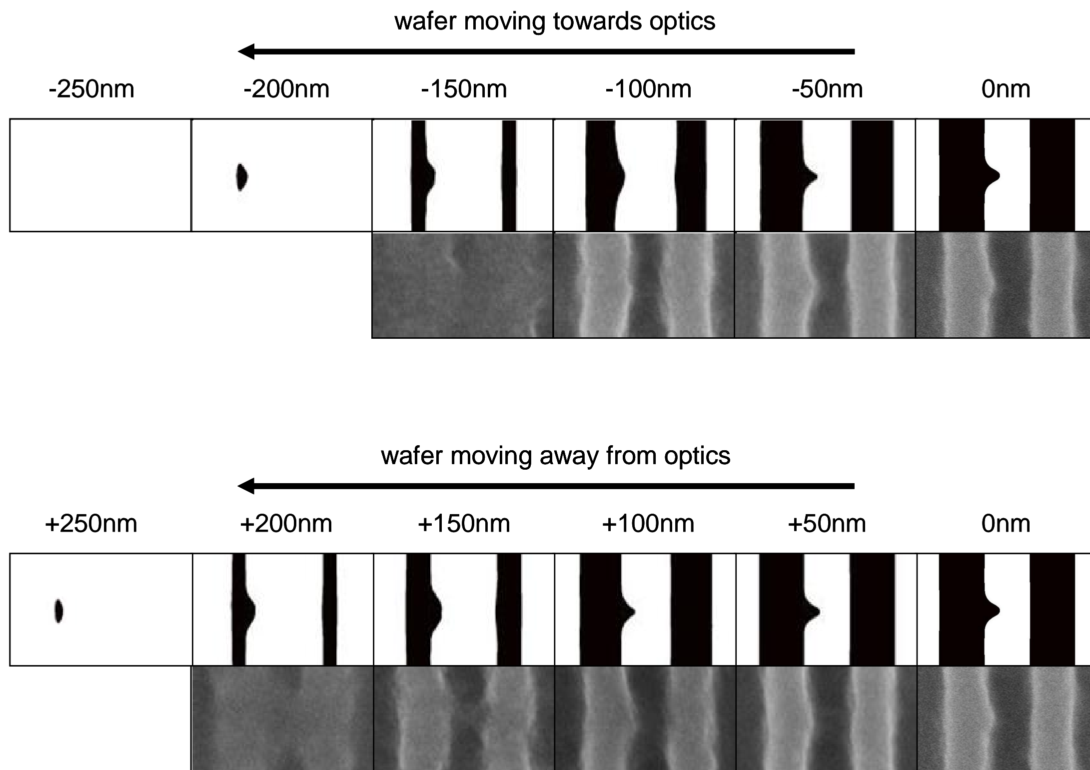

Fig. 7: Through-focus printing behavior of an exemplary defect in a dense line/space pattern (dark extension, 119 nm mask defect size). Note that the line/space pattern shows an opposite trend of the line CD vs defocus.

Finally, the through-focus behavior of the defect printing was investigated. Figure 7 compares the simulated aerial images with the actual wafer prints for an exemplary defect (line extension with 119 nm mask defect size (5x)). A change of the defect size is difficult to detect here since the boundaries of the resist features are blurred in the defocus. However, the CD change of the dense-line pattern through focus can be compared. For the simulations, the line CD is considerably reduced whereas the experimental data show a slight increase. This opposite trend of the CD vs defocus can be attributed to a shift of the iso-focal CD by the resist process due to an intrinsic bias. Such shift of the iso-focal CD was observed earlier under similar conditions for the same resist [5].

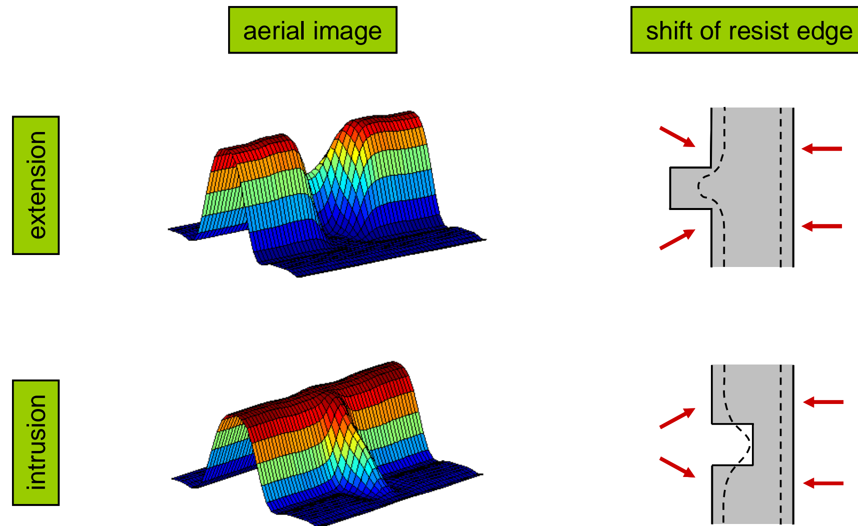

Fig. 8: Influence of the resist process on the resist shape of defects. Left side: aerial image of an extension and intrusion. Note that the high intensity corresponds to a space in resist. Right side: Sketch illustrating the shift of the pattern edges and smoothing in resist.

7. IMPACT OF THE RESIST PROCESS

In conclusion of the last section, all data reveal a strong impact of the resist process on the defect printability. The most obvious fact is the limitation of defect printing to defects larger than 100 nm on mask. The resolution of the lithographic process in general is driven by the resolution of both the projection optics (aerial image) and the resist process whatever might be limiting. This total resolution must be compared to the pattern to be printed. Features below the lithographic resolution capability are not printed although there is a gradual transition around the resolution limit.

On the wafer prints, the following observations are made: (1) small defects are resolved in the aerial image simulations but not in the printing, (2) the shape of printed defects is stretched parallel to the lines both for dark and clear defects, (3) the iso-focal CD is reduced in the wafer printing compared to simulation, and (4) the resolution limit of the MET-1K resist is approximately 30-40 nm (wafer scale) [7,8]. A comparison with the simulations of the aerial images leads us to conclude that the total resolution is not limited by the projection optics but by the resist process.

Transferring the aerial image into the chemically amplified resist means the following (see also Fig. 8): The exposure generates a concentration profile of photo acid in the resist roughly following the intensity distribution of the aerial image. Scattering and flare also generates small amounts of photo acid generally acting towards image degradation. The photo acid then starts diffusing proportionally to the concentration gradient especially during the post-exposure bake. In a balanced resist, the diffusion process can (partially) be counteracted by the proper amount of an added base (quencher).

In effect, the latent image in the resist is blurred and the edges of the developed resist are shifted with smoothing of the pattern shape (mask LER, corner rounding). These mechanisms of the resist process are here discussed qualitatively only. More details and quantitative discussions can be found in other publications [11,12].

These resist processes are capable of limiting the printed defect size. Whereas the CD change (bias) by the photo acid diffusion is experimentally adjusted by selecting the correct dose-to-size on the wafer, differences in contrast between the line/space pattern and the defects cannot be compensated for. In the aerial image, extensions of a line are not as dark as the line itself (and intrusions are not as bright as the space), i.e. the defects are much closer to the exposure threshold than the line/space pattern. The gradient in the corresponding concentration profile of the defects is smaller (less diffusion) but already relatively small change of the photo-acid concentration leads to a change of the printability. In particular, the defect shape is attacked on two sides in the vertical direction (upper and lower side) and on one side only in horizontal direction. Since point defects are considered, they do not print if the defect size is in the order of twice the diffusion length (unlike long defects used previously [3,4]).

8. SUMMARY

An EUV defect printability study of absorber point defects in a 60-nm line/space pattern (wafer scale) was carried out. The experimental results are compared to simulations of the aerial image. The simulations predict a linear scaling of the printed defect size with extensions of the absorber line being more critical than intrusions. Using a 10% criterion of acceptable CD variations the critical defect in simulation for the 60-nm design rule is 50 nm for extensions and 75 nm for intrusions.

The experimental printability in MET-1K resist is limited in our case to approximately 100 nm point defects on mask. For larger defects, extensions are found to be more critical than intrusions before they grow as much as to print as bridge defects or line breaks. Centered defects switch almost immediately between non-printing and bridging/line break. The strong differences between aerial-image simulation and experiment are explained by diffusion of the photo acid in the chemically amplified resist. The current resist process limits the defect printability of defects.

ACKNOWLEDGMENT

We would like to thank all people who contributed to this study. In particular we thank Patrick Naulleau and the staff at LBNL for the mask printing and Sven Trogisch, Markus Bender and Wolf-Dieter Domke for useful discussions. This work was partially funded by the German Federal Ministry of Education and Research (BMBF) under contract 01M3154A ("Abbildungsmethodiken für nanoelektronische Bauelemente"). AMTC is a joint venture of AMD, Inc., Infineon Technologies AG and Toppan Photomasks, Inc.

REFERENCES

1. International Technology Roadmap of Semiconductors, edition 2005. http://www.itrs.net/Common/2005ITRS/Home2005.htm
2. P.-Y. Yan, C.-W. Lai, and G. Cardinale, "EUV mask contact layer defect printability and requirement", *Emerging Lithographic Technologies IV*, Ed. E. Dobisz, Proc. SPIE **3997** (2000), pp 504-514.
3. J. Cobb, R. Peters, S. Postnikov, S. D. Hector, B. Lu, E. Weisbrod, J. Wasson, P. Mangat, and D. O'Connell, „Process latitude measurements and their implications for CD control in EUV lithography", paper 5374-5, *Emerging Lithographic Technologies VIII*, Ed. R. S. Mackay, Proc. SPIE **5374** (2004), pp. 43-52.
4. B. Lu, J. Wasson, P. Mangat, J. Cobb, S. D. Hector, D. Pettibone, and D. O'Connell, "Defect printability and Inspection of EUVL mask", paper 5567-162, *24th Annual BACUS Symposium on Photomask Technology*, Eds. W. Staud and J. T. Weed, Proc. SPIE **5567** (2004), pp. 1425-1434.
5. A. R. Pawloski, B. La Fontaine, H. J. Levinson, S. Hirscher, S. Schwarzl, K. Lowack, F.-M. Kamm, M. Bender, W.-D. Domke, C. Holfeld, U. Dersch, P. Naulleau, F. Letzkus, and J. Butschke, "Comparative study of mask

architectures for EUV lithography", paper 5567-82, *24th Annual BACUS Symposium on Photomask Technology*, Eds. W. Staud and J. T. Weed, Proc. SPIE **5567** (2004), pp. 762-773.

6. P. Naulleau, K. A. Goldberg, E. H. Anderson, K. Bradley, R. Delano, P. Denham, B. Gunion, B. Harteneck, B. Hoef, H. Huang, K. Jackson, G. Jones, D. Kemp, J. A. Liddle, R. Oort, A. Rawlins, S. Rekawa, F. Salmassi, R. Tackaberry, C. Chung, L. Hale, D. Phillion, G. Sommargren, and J. Taylor, "Status of EUV micro-exposure capabilities at the ALS using the 0.3-NA MET optic", paper 5374-135, *Emerging Lithographic Technologies VIII*, Ed. R. S. Mackay, Proc. SPIE **5374** (2004), pp. 881-894.
7. P. P. Naulleau, K. A. Goldberg, E. Anderson, J. P. Cain, P. Denham, K. Jackson, A.-S. Morlens, S. Rekawa, and F. Salmassi, "EUV microexposures at the ALS using the 0.3NA MET optic", paper 4C3, *48th International Conference on Electron, Ion and Photon Beam Technology and Nanofabrication*, J. Vac. Sci. Technol. B, **22** (2004), pp. 2962-2965.
8. P. Naulleau, C. Rammeloo, J. P. Cain, K. Dean, P. E. Denham, K. A. Goldberg, B. Hoef, B. La Fontaine, A. R. Pawloski, C. Larson, G. Wallraff, "Investigation of the current resolution limits of advanced EUV resists", paper 3IN11, *4th International Symposium on EUV Lithography*, San Diego, California (November 2005).
9. P. Evanschitzky and A. Erdmann, "Enhanced model for the efficient 2D and 3D simulation of defective EUV masks", paper 5374-88, *Emerging Lithographic Technologies VIII*, Ed. R. S. Mackay, Proc. SPIE **5374** (2004), pp. 770-779.
10. Database of optical constants, Center of X-ray Optics, Lawrence Berkeley National Laboratory. http://www-cxro.lbl.gov/optical_constants
11. W. Hinsberg, F. Houle, M. Sanchez, J. Hoffnagle, G. Walraff, D. Medeiros, G. Gallatin, and J. Cobb, "Extendibility of chemically amplified resists: Another brick wall?", paper 5039-1, *Advances in Resist Technology and Processing XX*, Ed. T. H. Fedynyshyn, Proc. SPIE **5039** (2003), pp. 1-14.
12. D. van Steenwinckel, J. H. Lammers, T. Koehler, R. L. Brainard, and P. Trefonas, „Resist effects at small pitches“, paper P19.4, *49th International Conference on Electron, Ion and Photon Beam Technology and Nanofabrication*, J. Vac. Sci. Technol. B, **24** (2006), pp. 316-320.